Midinfrared absorption of PbSe/$Pb_{1-x}Eu_xTe$ quantum dot superlattices in IV-VI microcavities

T. Schwarzl,[1,*] W. Heiss,[1] G. Springholz,[1] H. Krenn,[2] T. Fromherz,[1] A. Raab,[1] and I. Vavra[3]
[1]*Institut für Halbleiter- und Festkörperphysik, Johannes Kepler Universität Linz, Altenbergerstraße 69, A-4040 Linz, Austria*
[2]*Institut für Experimentalphysik, Karl-Franzens-Universität Graz, Universitätsplatz 5, A-8010 Graz, Austria*
[3]*Institute of Electrical Engineering, Slovak Academy of Sciences, 842 39 Bratislava, Slovakia*
(Received 20 February 2002; published 21 June 2002)

The midinfrared absorption of highly ordered self-assembled PbSe/$Pb_{1-x}Eu_xTe$ quantum dot superlattices is investigated. A different approach is used for quantitative determination of the absorption spectrum of the dot superlattice by inserting it into a high-finesse microcavity structure with a small mode spacing and $Pb_{1-x}Eu_xTe$/EuTe Bragg mirrors. For such microcavities, we show a linear relation between the width of each cavity resonance and the extinction coefficient at the resonance energy. Thus, the absorption spectrum is experimentally determined from the resonance widths. It reveals a narrow peak arising from the quantum dots and a step from the two-dimensional wetting layers. The peak absorption coefficient of the dot ensemble amounts to 2.5×10^4 cm^{-1} and is similar to that of the wetting layers. We also present calculations of the dispersion of the absorption coefficient based on model dielectric functions of quantum dots and wetting layers. From a fit to the experimental absorption spectrum, we deduce interband transition energies as well as corresponding oscillator strengths and level broadenings. The broadening of the dot transition due to dot size fluctuations of the large quantum dot ensemble is only 8.7 meV, confirming the exceptionally high dot size uniformity in the PbSe quantum dot superlattice.

DOI: 10.1103/PhysRevB.65.245321 PACS number(s): 78.67.Hc, 78.20.Ci, 78.30.Hv, 78.67.De

I. INTRODUCTION

Nowadays a great deal of research in semiconductor physics is devoted to systems with reduced dimensionality. This is due to the multifaceted physical effects originating from the energy quantization that can be found in such systems, which has led, e.g., to drastic improvement of optoelectronic devices.[1] In particular, reducing the dimensionality to zero so that free carriers are confined in all three directions results in an atomlike density of states with δ spikes at the energy levels.[2–4] Such, quantum dots have been employed to reduce the threshold in semiconductor lasers significantly.[1,5]

Several semiconductor processing methods have been used for the fabrication of zero-dimensional (OD) structures. One method is the direct synthesis of self-assembled dots by the Stranski-Krastanow growth, which yields defect-free quantum dots[6,7] as is essential for device applications.[8,9] This approach is based on heteroepitaxy of highly strained layers, leading to spontaneous formation of nanometer-sized coherent islands on the epitaxial surface. The island formation starts at a certain critical layer thickness and is driven by the strong reduction of strain energy allowed by the growth of such freestanding islands. For highly strained layers, this reduction of strain energy by far outweighs the increase in free-surface energy. Thus, defect-free islands are gained. When embedded in a higher band-gap matrix material, such self-assembled quantum dots have shown excellent electronic properties due to the effective confinement of free carriers.

For practical applications of self-assembled quantum dots in devices such as quantum dot lasers performance limitations were observed due to the size and shape variations of large dot ensembles, leading to a considerable inhomogeneous broadening of the luminescence emission lines as compared to the sharp almost δ like emission found from the studies on single dots.[6] Therefore, the improved size homogeneity found in multilayers or superlattices of self-assembled quantum dots due to the ordering of the dots induced by their interactions via their elastic strain fields has recently become an object of intense study.[10–12] We have applied this concept to molecular-beam epitaxy (MBE) of IV-VI semiconductor compounds[13] demonstrating a very high size homogeneity caused by the efficient lateral as well as vertical ordering in PbSe/$Pb_{1-x}Eu_xTe$ quantum dot superlattices.[14,15] As a result, three-dimensional quantum dot crystals were obtained with the dots arranged in a trigonal lattice with face-centered-cubic-like *A-B-C-A-B-C-* $\cdots$ vertical stacking sequence and a *tunable* lattice constant.[14–16] This quantum dot arrangement is unique to the IV-VI compounds due to their high elastic anisotropy, which strongly influences the elastic interaction between the growing dots on the surface and those buried in the previous superlattice layers.[17]

Due to the narrow size distribution and the excellent control of the absolute size as well as lateral distance of the dots, our PbSe dot superlattices are major candidates for optoelectronic applications where precise tuning of the optical and electronic properties is of crucial importance. Owing to their narrow-band gaps, all IV-VI semiconductors (lead salt compounds) show emission in the midinfrared range, and have thus been widely applied for fabrication of midinfrared diode lasers[18–21] and detectors[22] for high-resolution gas spectroscopy and analysis. Although much progress has been achieved with long-wavelength III-V quantum cascade lasers and type II antimonide lasers,[23–25] electrically pumped lead salt lasers are still the only commercially available semiconductor laser sources for the 3–5 μm range. This is due to the facts that the IV-VI compounds exhibit nearly symmetric conduction and valence bands at the direct energy-band gap

and up to two order of magnitude lower Auger recombination rates than for InSb or HgCdTe of comparable values for the band-gap.[26]

In the present work, we have studied the dispersion of the absorption coefficient of $PbSe/Pb_{1-x}Eu_xTe$ quantum dot superlattices. For these structures, grown on transparent BaF_2 substrates, the absorption of the dots is not directly accessible by simple transmission and reflectivity measurements due to the pronounced multiple reflection interference fringes in the optical spectra. These interference fringes are caused by the large difference in the refractive indices of the IV-VI layers and the BaF_2 substrate. As a remedy to these problems, we have applied IV-VI-based ultra-high-finesse microcavities for the midinfrared[27] as optical probe for the PbSe quantum dot superlattices. Microcavities with high-reflectivity Bragg interference mirrors and a length comparable to the optical wavelength have met immense interest in the last few years owing to their unique physical properties such as the appearance of cavity polaritons[28] and their high potential for device applications.[29] Here, we have used microcavities similar to those employed for the fabrication of midinfrared IV-VI vertical-cavity surface-emitting lasers (VCSELs)[30–33] operating in pulsed mode up to 65 °C.[32]

For quantitative investigation of the midinfrared absorption of the dots inside the cavity, we have developed a different method based on the evaluation of the width of the cavity resonances. From theoretical calculations, this width is shown to depend linearly on to the absorption of the materials inside the cavity. This approach is then applied to microcavities filled with an ordered PbSe quantum dot superlattice for quantitative experimental determination of the dispersion of the quantum dot absorption coefficient in the spectral range of the stop band of the cavity Bragg mirrors. The experimental findings are compared to theoretical calculations, which unambiguously confirm that the measured absorption arises from 0D (quantum dot) and 2D (wetting layer) systems. These calculations are based on a model for the dielectric function of bulk lead salt materials,[34] which is extended here to cover also low dimensional structures. From our absorption measurements, we find a very narrow spectral width of the PbSe quantum dot absorption peak of only 9 meV due to the exceptionally narrow size distribution of the dots. Finally, our results are also compared to recent optical studies on spherical IV-VI nanocrystals in glass matrices.[35,36]

II. SAMPLE STRUCTURE AND EXPERIMENT

The high-finesse IV-VI microcavity samples filled with the PbSe quantum dot superlattice were grown by MBE onto (111) oriented BaF_2 substrates using compound effusion cells for PbTe and PbSe, and elemental sources for Eu and Te. The Eu concentration in the ternary $Pb_{1-x}Eu_xTe$ was adjusted by the ratio of the PbTe to the Eu beam flux with an excess Te_2 flux for a correct stoichiometry. The pyramidal shaped self-organized PbSe quantum dots were formed during Stranski-Krastanow heteroepitaxial growth of PbSe on PbEuTe due to the 5.4% lattice mismatch.[15,16] The dot superlattices were grown at 360 °C deposition temperature by alternating 5 monolayers (ML) of PbSe with 480-Å $Pb_{1-x}Eu_xTe$ spacer layers on a $Pb_{1-x}Eu_xTe$ buffer layer with growth rates of 0.13 ML/s and 4.9 Å/s for PbSe and $Pb_{1-x}Eu_xTe$, respectively. Under these conditions, the dots in the superlattice are aligned in directions inclined by about 39° to the growth direction and thus, form a nearly perfect 3D lattice with fcc-like *ABC-ABC-*$\cdots$ stacking.[14] An areal dot density of about 250 μm^{-2} (lateral separation 680 Å), an average dot height of 120 Å, and a base width of 300 Å with a relative full width at half maximum of the dot size distribution of about $\pm 10\%$ is observed for superlattices with more than 60 bilayers.[15,16] The strong increase of the band-gap energy of $Pb_{1-x}Eu_xTe$ with increasing Eu content[37] and the larger band gap of PbTe as compared to PbSe lead to a significant quantum confinement of the free carriers in the PbSe dots. In bulk material, the energy gaps at 4 K amount to 422 meV and 146 meV for $Pb_{0.95}Eu_{0.05}Te$ and PbSe, respectively.[34]

The dot superlattice is sandwiched between two high-reflectivity Bragg mirrors each consisting of 3 periods of quarter wavelength $EuTe/Pb_{0.94}Eu_{0.06}Te$ bilayers with a thickness of 5130 Å and 2530 Å for EuTe and $Pb_{1-x}Eu_xTe$, respectively. The mirrors were grown at a temperature of 260 °C in order to achieve two-dimensional growth for EuTe.[38] Because only one Eu effusion cell was available in the MBE system the $Pb_{0.94}Eu_{0.06}Te$ mirror layers were deposited as short period superlattices of 40 Å PbTe alternating with 13 Å $Pb_{0.7}Eu_{0.3}Te$. Due to the very high refractive index contrast between $Pb_{1-x}Eu_xTe$ and EuTe ($n_{EuTe}=2.3$ and $n_{Pb_{1-x}Eu_xTe}=5.5$), a mirror reflectivity exceeding 99% is achieved. This is essential for obtaining a cavity with a high finesse.[27,31–33]

Figure 1(b) shows a cross-sectional scanning electron microscope (SEM) image of the complete microcavity structure with a 10-μm-thick cavity filled with a 3-μm $Pb_{1-x}Eu_xTe$ buffer layer and a 140-period $PbSe/Pb_{1-x}Eu_xTe$ quantum dot superlattice. The material contrast between the different layers was enhanced by selective plasma etching.[39] The unique ordering of the dot superlattice in the cavity is revealed by the transmission electron microscope (TEM) image in Fig. 1(a), clearly showing the inclined dot alignment (see dashed lines). Apart from these microcavity samples, we have also investigated the optical transmission of PbSe quantum dot superlattice reference samples without a microcavity structure.

Midinfrared transmission measurements of the samples at temperatures between 20 K and 300 K were performed using a Bomem DA8 Fourier-transform spectrometer with a continuous flow He cryostat and InSb as well as HgCdTe detectors.

III. THEORETICAL APPROACH FOR EVALUATING THE ABSORPTION IN A MICROCAVITY

For the determination of the dot absorption, an important approach for evaluating the dispersion of the absorption coefficient of materials placed inside a thick microcavity with a

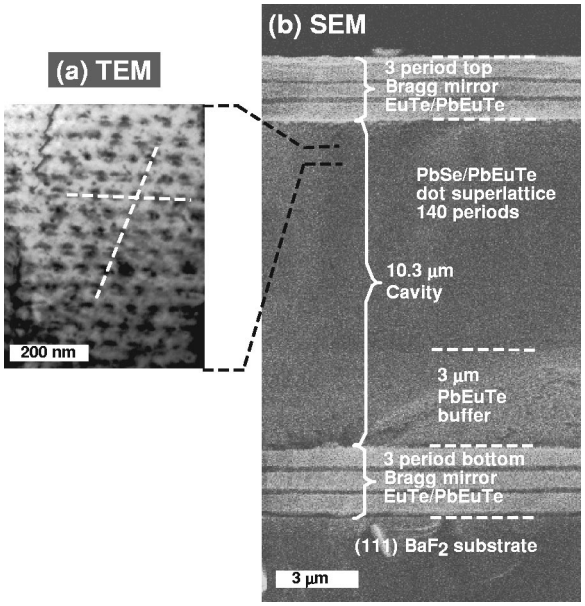

FIG. 1. (a) Cross-sectional TEM image of the PbSe/$Pb_{1-x}Eu_xTe$ quantum dot superlattice inside a microcavity showing the ordering of the dots. (b) Cross-sectional SEM image of the complete microcavity structure (1220) consisting of two 3-period EuTe/$Pb_{1-x}Eu_xTe$ Bragg mirrors and a 10-μm-thick cavity filled with the 140-period PbSe/$Pb_{1-x}Eu_xTe$ quantum dot superlattice. The sample structure is indicated in the image.

small spacing of the cavity resonances and a high finesse is used. In this case, the light confined in the resonator is strongly enhanced due to the high quality factor of the cavity, and thus a high sensitivity for the determination of the cavity absorption is gained. Our approach is based on measuring the full width at half maximum w of all cavity modes, which linearly depends on the imaginary part of the refractive index of the cavity materials. The imaginary part of the refractive index (the extinction coefficient κ) is responsible for absorption in a medium. κ is directly related to the absorption coefficient α via

$$\alpha = \frac{4\pi\kappa}{\lambda}, \tag{1}$$

where λ denotes the wavelength of the light in vacuum. Thus, we can extract the absorption coefficient from the width w of a cavity mode at the energy position of this mode. The mode spacing of the microcavity is, therefore, the resolution for the energy dispersion of α.

Figure 2 shows the transmission as calculated by the transfer-matrix method[40] for a thick high-finesse microcavity incorporating an absorber without any spectral dispersion. The cavity structure consists of high reflectivity EuTe/$Pb_{1-x}Eu_xTe$ Bragg mirrors[27] and a rather large thickness of 10 μm, as described in Sec. II. The transmission spectrum exhibits a broad mirror stop band with essentially zero transmission from 204 meV to 366 meV and with 17

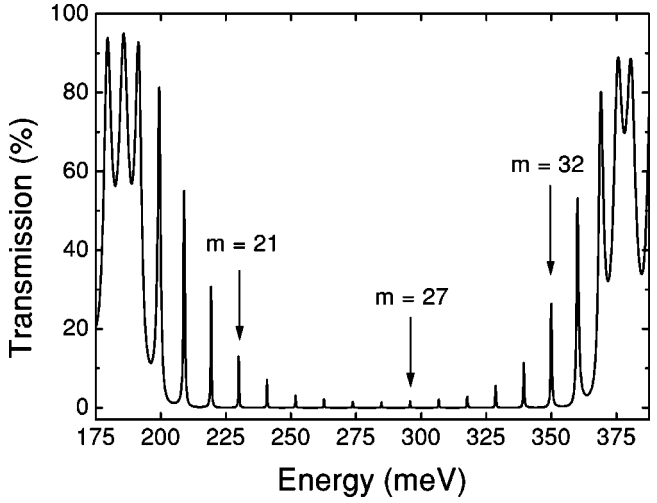

FIG. 2. Calculated transmission spectrum of a thick high-finesse microcavity with an absorber without dispersion in it in the region of the Bragg mirror stop band. The order m of three cavity resonances is indicated.

narrow cavity resonance peaks in it. The cavity mode spacing is only 10 meV due to the large thickness of the resonator.

The influence of the extinction coefficient κ of the cavity material on an individual cavity resonance is plotted in Fig. 3 for the mode with the order $m=21$. It is clearly seen that the resonance width (dotted lines) is increasing and the resonance height is decreasing due to enhanced damping with increasing κ. The peak transmission shows a strongly nonlinear behavior on κ, but the resonance width increases almost linearly with increasing values of κ. Therefore, it is convenient to use the width to extract the extinction coefficient. This is shown in Fig. 4(a), by plotting the width w of three different resonances ($m=21$,27, and 32, see arrows in Fig. 2) as a function of κ. The width w is taken from a

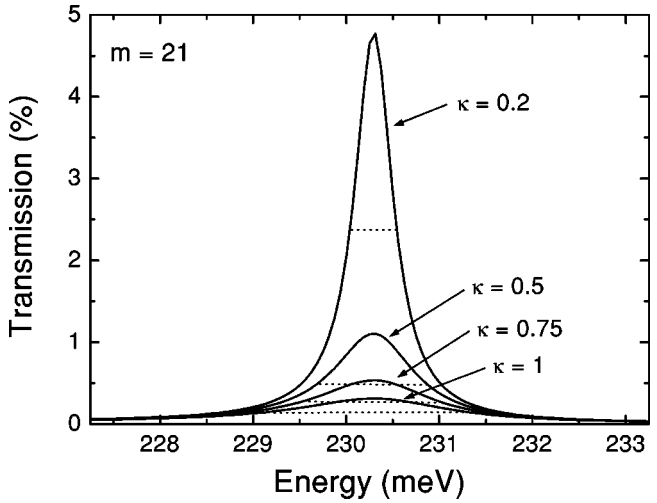

FIG. 3. Calculated transmission of the 21st-order cavity resonance of the microcavity in dependence of the extinction coefficient κ of the cavity material. The width of the resonances is indicated by the dashed lines.

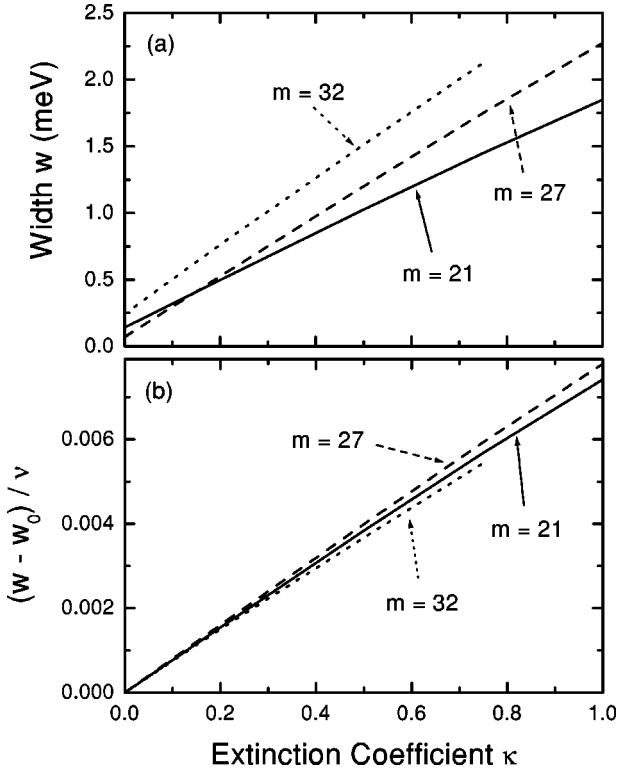

FIG. 4. (a) Calculated width w of three cavity resonances of the order of $m=21,27$, and 32 as a function of the extinction coefficient κ. (b) Calculated normalized change in resonance width $(w-w_0)/\nu$ for the three resonances as a function of κ.

Lorentzian fit to the resonance peaks, and indeed for all three modes we find a linear relation between w and κ. However, the slope is notably different for the various modes. This is due to the fact that the cavity mirror reflectivity is still energy dependent inside the stop band (it is highest in the center of the stop band, see, for instance, Ref. 27). Since each individual resonance width is directly connected to the reflectivity at the resonance position ν, the modes do not exhibit (even for $\kappa=0$) the same line broadening over the full stop band width. In addition, the absolute resonance width w increases for modes at higher energies proportional to the mode energy ν. To take these factors into account, we plot in Fig. 4(b) the *change* in the relative resonance width (w/ν) with respect to the width (w_0/ν) for $\kappa=0$ as a function of κ. Clearly, this normalized change in resonance width $(w-w_0)/\nu$ shows the same linear dependence on the extinction coefficient for all three resonances with a slope of 7.5×10^{-3}. Therefore, using the resonance widths of the undamped cavity as a reference, the extinction coefficient κ can be directly deduced from the measured cavity resonance widths using Fig. 4(b). The small remaining deviation at large κ in Fig. 4(b) arises from the inaccuracies of the Lorentzian line fits to the resonances, especially near the edges of the mirror stop band where the transmission starts to increase. Our theoretical analysis demonstrates that in thick microcavities it is possible to determine quantitatively the energy dispersion of the extinction coefficient κ of the cavity materials within the Bragg mirror stop band region by measuring the normalized change in resonance width $(w-w_0)/\nu$ of all microcavity resonances.

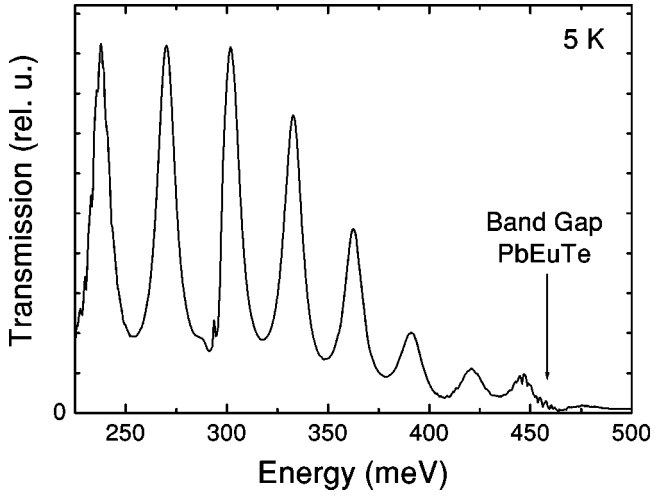

FIG. 5. The FTIR transmission spectrum of a 30-period reference $PbSe/Pb_{1-x}Eu_xTe$ quantum dot superlattice (972) at 5 K.

IV. RESULTS AND DISCUSSION

A. Transmission measurements of a reference quantum dot superlattice

For practical applications of quantum dot superlattices, it is essential to know the optical density of the dots. For that purpose, we first measured the Fourier-transform infrared (FTIR) transmission spectrum at 5 K of a 30-period reference superlattice (sample 972), as shown in Fig. 5. In this low-temperature transmission spectrum, an absorptive region can be observed above an energy of about 320 meV. The energy-band gap of the $Pb_{1-x}Eu_xTe$ buffer and spacer layers is revealed by the transmission cutoff at about 460 meV. A detailed analysis of the dispersion of the absorption from the quantum dots is obviously not possible from such measurements due to the strong interference fringes inherent in the transmission spectrum. These interference fringes and their strong dispersion arise from the exceptionally high refractive index of about 5–6 for the lead salt materials as compared to $n=1.4$ of the transparent BaF_2 substrate, which leads to the strong multiple reflections at the layer/air and layer/substrate interfaces. Therefore, we used the approach described in Sec. III for the determination of the dispersion of the absorption coefficient. This is outlined in the following section.

B. Evaluation of the PbSe quantum dot absorption in a microcavity

To gain direct access to the extinction coefficient and ultimately to the absorption coefficient, we place the quantum dot superlattice in a thick high-finesse microcavity (sample 1220) as described in Sec. II. According to Sec. III, the normalized change in resonance width $(w-w_0)/\nu$ of all microcavity resonances has to be gathered. Thus, the width w of the cavity resonances with the absorbing quantum dot superlattice inside the cavity as well as the reference widths w_0 of

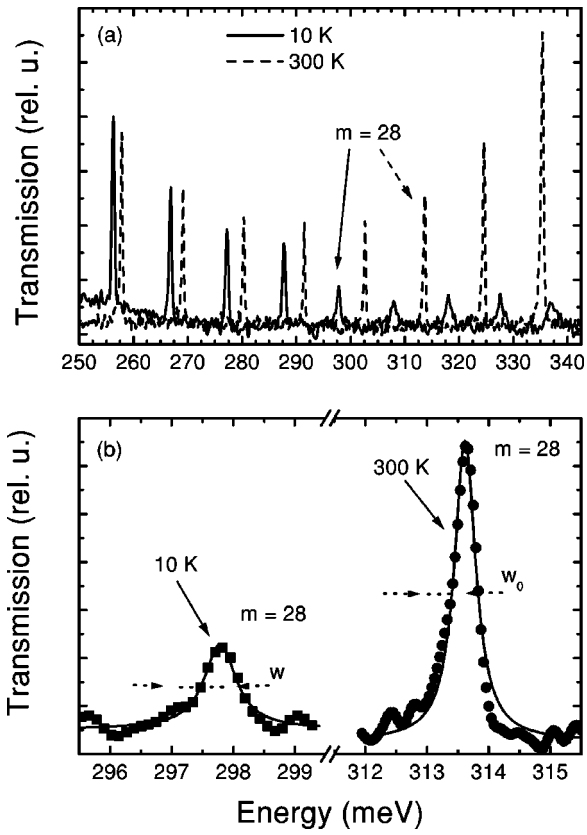

FIG. 6. The FTIR transmission spectrum of the quantum dot cavity (1220) at 10 K (full line) and 300 K (dashed line). Only the central energy region of the Bragg mirror stop band is shown.

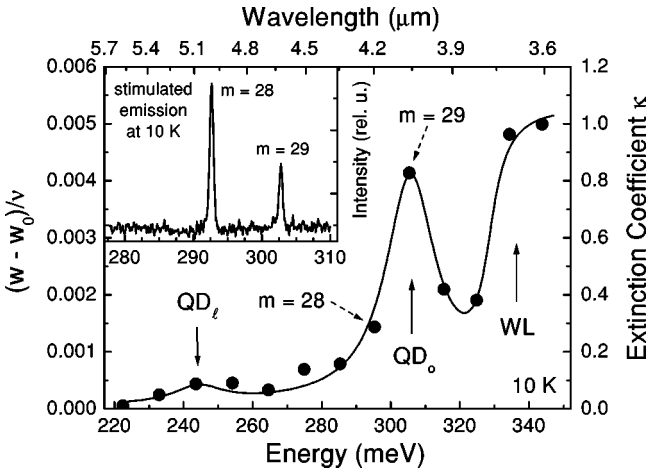

FIG. 7. Dispersion of the extinction coefficient κ of the quantum dot superlattice at 10 K. Left-hand scale: normalized change in resonance widths $(w-w_0)/\nu$ for all resonances of the quantum dot cavity (1220) vs resonance position ν (filled dots). Right-hand scale: corresponding values for the extinction coefficient (see text). The full line shows the fitted calculation of the dispersion of the extinction coefficient. Inset: Stimulated VCSEL emission spectrum at 10 K from the same sample consisting of two laser lines corresponding to the cavity resonances with the orders $m=28$ and 29 (indicated as dashed arrows in the main figure).

the same cavity but without an absorber inside have to be measured. This is peformed by high-resolution transmission measurements of the cavity at two different temperatures of 10 K and 300 K. From the room-temperature spectrum, we gather the reference widths w_0 without absorption in the cavity. This is possible because the energy-band gap of the IV-VI materials strongly increases with temperature [e.g., the band-gap of PbSe increases from 146 meV at 4 K to 276 meV at 300 K (Ref. 34)]. Therefore, at room temperature any absorption is shifted well above the stop band range so that the resonances at 300 K are virtually free of absorption This is also evidenced by room-temperature transmission measurements of the bare reference quantum dot sample. At low temperatures, the onset of the dot absorption is near the stop band center, i.e., the higher resonances become strongly damped and thus, the dot absorption can be obtained. Therefore, both quantities w and w_0 required for our analysis are extracted from the *same* sample.

The measured transmission spectra are similar to the calculated spectrum of Fig. 2, showing a broad Bragg mirror stop band region of zero transmission and many narrow resonance peaks in the stop band. For clarity, only the central energy region of the stop band is plotted in the FTIR transmission spectra of Fig. 6(a) at 10 K (full line) and 300 K (dashed line) depicting the central resonances clearly. It is important to point out that the energetic position of the cavity modes is different at each temperature, which has to be taken into account when evaluating $(w-w_0)$ for a certain resonance. For example, the 28th-order resonance mode at 10 K and 300 K [see arrows in Fig. 6(a)] are about 16 meV apart. This is due to the fact that the effective refractive index of the cavity material slightly decreases with increasing temperature. A definite assignment of mode numbers is possible from transfer-matrix calculations as performed in Sec. III.

A comparison of the spectra at the two temperatures shows that at 10 K the resonances above 290 meV are considerably damped and broadened. This indicates an absorption in that region. In Fig. 6(b) the 28th-order mode at 10 K and 300 K is shown in an enlarged scale, clearly revealing the damping and broadening of the 10 K mode as compared to the undamped mode at room temperature. Both resonances are fitted with a Lorentzian line shape function [full lines in Fig. 6(b)], from which the widths w and w_0 are deduced. The same procedure is carried out for all other cavity modes. The result of the normalized change in resonance widths $(w-w_0)/\nu$ for all resonances is plotted in Fig. 7 as filled dots (left-hand scale) vs resonance position ν. The values for the normalized widths were transformed to the extinction coefficient κ using Fig. 4(b). The resulting quantitative values of κ, corresponding to the measured resonance peak widths, are depicted on the right-hand scale of Fig. 7. Thus, Fig. 7 represents the energy dispersion of the extinction coefficient of the quantum dot superlattice.

The absorption spectrum clearly shows an absorption peak around an energy of 305 meV (4.06 μm) and a steplike increase at 328 meV (3.77 μm). The peak, corresponding to an absorption coefficient $\alpha=2.5\times10^4$ cm^{-1}, is attributed to absorption from the dot ensemble, whereas the step ($\alpha=3.3\times10^4$ cm^{-1}) is attributed to the wetting layers, because of the distinct 0D- and 2D-like behavior, respectively. The value of the wetting layer absorption matches quite well

with the absorption measured in IV-VI multi-quantum-well structures.[41] The results also fit very well to our results on quantum dot (QD) VCSEL emission from the same structure (see Ref. 33). The laser emission spectrum at 10 K is depicted in the inset of Fig. 7 and shows two laser lines at the position of the 28th- and the 29th-order resonance modes that are also the first two modes contained in the quantum dot absorption peak around 305 meV (see dashed arrows in Fig. 7). Furthermore, an additional absorption peak of the same width as that of 305 meV is found at an energy of about 248 meV (5 μm). Considering the many valley band structure of the lead salt compounds with one longitudinal valley along the (111) growth direction and three oblique valleys inclined by 70.53° to the growth direction,[42] this peak can be attributed to optical transitions in the longitudinal valleys (thus labeled QD_l), whereas the strong peak at 305 meV arises from the oblique valleys (labeled QD_o). The smaller absorption in the longitudinal valley is due to the corresponding smaller oscillator strength as compared to the oblique valleys.[41] We have to point out, however, that this shift between QD_l and QD_o presumes that the dots in the superlattice have a flattened shape, and that the valley degeneracy is lifted as observed in 2D systems.[41,43] This assumption is based on the general observation of a flattening of the dot shapes during overgrowth.[44] Because the quantization energies of the dots depend inversely on the effective masses, our assignment is supported by the fact that the ratio of the energy positions of the quantum dot absorption peaks approximately corresponds to the ratio of the longitudinal and transversal effective masses of PbSe.[34] In this picture, the mentioned quantum dot VCSEL emission[33] stems only from transitions in the oblique valleys. This agrees with our previous results on IV-VI VCSELs with *quantum wells* as active region.[31,32]

In principle, a higher energy resolution of the absorption measurement can be achieved by increasing the cavity thickness and thus decreasing the cavity mode spacing. However, fabrication of samples with thicknesses much exceeding 10 μm is rather time consuming for MBE, but any other growth technique could be used as well for that purpose.

C. Calculation of the quantum dot absorption

For an unambiguous confirmation of the interpretation of our experimental results, we have investigated the absorption spectrum of the IV-VI quantum dot superlattice theoretically by calculating the dielectric function of the dots, the wetting layers, and the spacer layers in the superlattice. Parameters such as transition energies and level broadening as well as oscillator strengths were determined by fits to the experimental absorption spectrum.

The calculation is based on a model for the complex dielectric function ϵ of the lead salts,[34] which includes the nonparabolicity of the band structure near the energy-band gap as well as the anisotropic many valley band structure of the lead salt compounds. The imaginary part of the dielectric function $\mathrm{Im}(\epsilon)$ is determined in terms of joint density of states between valence and conduction bands. In order to obey the causality principle between the optical constants, the real part of the dielectric function $\mathrm{Re}(\epsilon)$ is calculated by a Kramers-Kronig transformation. The Kramers-Kronig integral can be evaluated *analytically* because level broadening is introduced *after* the transformation. This is done by continuing the photon energy E in $\mathrm{Re}(\epsilon)$ into the complex plane by adding an imaginary damping parameter $i\Gamma$, and thus, gaining a closed expression for the full complex dielectric function. The derivation was performed in detail for 3D bulk PbSe in Ref. 34. In order to obtain expressions for $\epsilon(E)$ valid for the 2D wetting layers and 0D quantum dots, the joint density of states for a 2D and a 0D system have to be calculated. For a 2D system, this is performed in Ref. 45, resulting in the following dielectric function:

$$\epsilon_{2D}(E)=A_i\frac{E_i}{(E+i\Gamma_{2D})}\ln\left(\frac{E+i\Gamma_{2D}+E_i}{E+i\Gamma_{2D}-E_i}\right), \tag{2}$$

in which A_i means a dimensionless parameter interpreted as the oscillator strength for 2D interband transitions and E_i the energy of the corresponding transitions. The oscillator strengths for oblique (o) and longitudinal (l) transitions are given by[45]

$$A_o=\frac{e^2}{2\pi\epsilon_0}\left(4\frac{2P_\parallel^2}{m_0}+5\frac{2P_\perp^2}{m_0}\right)\frac{M_\perp}{m_0}\sqrt{\frac{M_\parallel}{M_\parallel+8M_\perp}}\frac{1}{E_o^2}\frac{1}{d}, \tag{3}$$

$$A_l=\frac{e^2}{2\pi\epsilon_0}\frac{2P_\perp^2}{m_0}\frac{M_\perp}{m_0}\frac{1}{E_l^2}\frac{1}{d}. \tag{4}$$

In these expressions, $P_\perp$ and $P_\parallel$ are the transverse and longitudinal momentum matrix elements, respectively, $M_\perp$ and $M_\parallel$ the corresponding density-of-states masses, m_0 the free-electron mass and d the thickness of the 2D quantum-well layers.

The dielectric function of the quantum dots ϵ_{0D} was derived as in Ref. 46, but considering the dot size dispersion by introducing level broadening with the damping parameter Γ as described above instead of using a Gaussian dot size distribution as in Ref. 46. Also the non-degeneracy between oblique and longitudinal valleys expected for flattened dots, as outlined in Sec. IV B, was included. Thus, we found the following expression for $\epsilon(E)$ valid for 0D quantum dots:

$$\epsilon_{0D}(E)=B_i\frac{E_i^3}{E_i^3-E_i(E+i\Gamma_{0D})^2}. \tag{5}$$

Similar to Eq. (2), B_i is a dimensionless parameter interpreted as the oscillator strength for 0D interband transitions and E_i the energy of the corresponding transitions. The oscillator strengths for oblique and longitudinal transitions are given by

$$B_o=\frac{4e^2\hbar^2}{3\epsilon_0 m_0}\left(4\frac{2P_\parallel^2}{m_0}+5\frac{2P_\perp^2}{m_0}\right)\frac{1}{E_o^3}\frac{1}{V}, \tag{6}$$

$$B_l=\frac{4e^2\hbar^2}{\epsilon_0 m_0}\frac{2P_\perp^2}{m_0}\frac{1}{E_l^3}\frac{1}{V}, \tag{7}$$

TABLE I. Fit parameters of the model dielectric functions for quantum dots and wetting layers [Eqs. (2) and (5)] to the experimental absorption spectrum of the $PbSe/Pb_{1-x}Eu_xTe$ quantum dot superlattice. For the oscillator strengths A and B of wetting layers and dots, respectively (A_o, B_o for the oblique valleys, B_l for the longitudinal valley), also the theoretical values calculated from Eqs. (3), (6), and (7) using the PbSe band parameters[34] are given for comparison. Γ is the damping of the optical transitions at the energies E_o and E_l for the oblique and longitudinal valleys, respectively.

	$B_{o,fit}$	$B_{l,fit}$	$A_{o,fit}$	$B_{o,theor}$	$B_{l,theor}$	$A_{o,theor}$	Γ (meV)	E_o (meV)	E_l (meV)
Dots	0.42	0.041		0.373	0.3		8.7	305	244
Wetting layer			4.65			4.82	3.7	328	

where V is the volume of the quantum dots.

With the given expressions, we are able to calculate the absorption spectrum of the quantum dot superlattice using the transfer-matrix method. To employ this method, we treated the dot layers (complex refractive index n_{0D}) overgrown with the spacer material (complex refractive index n_{3D}) as an effective medium consisting of a 0D and a 3D system. The portion of the 0D dot material in the effective medium was determined by the ratio of the average height of the buried dots h (about 100 Å) and the nominal thickness d_{dot}(7 Å) of the PbSe dot material if the latter is viewed as homogeneously distributed over the sample area. The latter value is known from the growth parameters. From these values a filling factor F of the dot material in the effective medium is calculated as $F=d_{dot}/h$. Thus, the complex refractive index n_{eff} of the effective medium is expressed as

$$n_{eff}=Fn_{0D}+(1-F)n_{3D}. \tag{8}$$

The result of the fit to the experimental absorption spectrum using the transition energies E_i, damping parameters Γ and oscillator strengths A_i,B_i as fitting parameters (quantum dots: oblique and longitudinal transition, wetting layer: oblique transition) is shown in Fig. 7 as the full line. Evidently, the calculated fit agrees very well with the experimental data. It is emphasized that the determination of the fitting parameters is easily accomplished and unambiguous. The resulting quantities for quantum dots (oblique and longitudinal transition) and wetting layer (oblique transition) are summarized in Table I, together with the values for the oscillator strengths obtained from Eqs. (3), (6), and (7) using the band parameters of PbSe at 4.2 K from Ref. 34 and the values of the dot volume and the thickness of the wetting layer of 4500 nm^3 and 11 Å, respectively. The agreement between fitted and theoretical values is notably good, especially for the oscillator strength A of the wetting layers with an error of less than 4%. This is an additional indication that our approach to extract the absorption from the widths of the cavity resonances is reasonable. However, the theoretical value for the longitudinal oscillator strength of the dots differs from the experimental result by a factor of 7. This indicates that the electronic wave functions in the dots differ significantly from those in bulk PbSe. Thus, it is not surprising that the used bulk matrix elements in the calculations do not yield an accurate value for the smaller absorption of the longitudinal valley in the dots.

The attribution of the absorption features to dots and wetting layers is further confirmed by the fact that the broadening Γ of the transition in the wetting layers of 3.7 meV is much smaller than that of the dots (8.7 meV). In contrast to a 0D system, in a 2D system fluctuations of the confining thicknesses are only possible in one direction instead of three. Therefore, a smaller broadening of transitions in 2D systems is expected as compared to the case in 0D systems. For absorption measurements on IV-VI multi-quantum-well structures of well widths 62–118 Å, a typical broadening of the optical transitions of 1.2 meV was found.[41] Taking into account the much smaller thickness of our wetting layer (11 Å), the broadening values agree reasonably well.

The remarkably small broadening of 8.7 meV of the quantum dot absorption peak clearly reflects the very high size homogeneity of the dot ensemble in our superlattices. From this broadening, the effective size distribution of the dots is estimated to be smaller than $\pm 3\%$, which is significantly below the value of $\pm 10\%$ obtained from atomic force microscopy measurements of the height distribution of free-standing dots on top of the superlattice.[15] For comparison, in spherical PbSe nanocrystal quantum dots in a glass matrix, a size distribution of $\pm 7\%$ determined from absorption measurements (absorption peak width of around 25 meV) was found.[35,36] A direct comparison of our dot absorption coefficients with those of the PbSe nanocrystals in a glass matrix is not possible because no quantitative values were given for these dots.[35,36] Self-assembled, Stranski-Krastanow grown quantum dots in other material systems such as InAs/GaAs,[2,47–50] $In_{1-x}GaAs_x/GaAs$,[6,51,52] $Al_{1-x}In_xAs/Al_{1-x}Ga_xAs$,[4] Ge/Si[53,54] usually show a much broader photoluminescence (PL) emission of the order of 50 meV due to the statistical dot size variations.[2] Quantum dot formation in CdTe/ZnTe superlattices[55] leads to a PL emission line width of about 20 meV. Even in III-V dot superlattices with ordering and size homogenization due to the vertical dot alignment[10–12,48–52] the best quantum dot PL peak width is not below 22 meV.[49] Thus, it is concluded that the dot size distribution in our PbSe dot superlattice is exceptionally narrow due to the highly efficient ordering mechanism during growth.[14]

As a further self-consistency check, we have calculated the cavity resonance widths using the measured dot superlattice absorption spectrum of Fig. 7 as input parameter instead of a frequency-independent absorption as used for Fig. 4. The such calculated widths agree well with the measured values, with only a slight readjustment of the mapping of the

change of the resonance widths $(w-w_0)/\nu$ onto the extinction coefficient κ [Fig. 4(b)]. This clearly shows that no coupling process of the cavity resonances to the probed optical transitions takes place, since the broadening of the transitions were exactly reproduced by this cross-check. In fact, this result was expected because the width of the quantum dot absorption is not only considerable broader than the widths of the cavity resonances but also broader than the cavity mode spacing. Thus, the coupling of the cavity to the dot transition is too weak to show a cavity polariton effect.[56]

V. CONCLUSION

In summary, we have determined the optical absorption spectrum of highly ordered self-assembled $PbSe/Pb_{1-x}Eu_xTe$ quantum dot crystals. Due to the large refractive index mismatch of the IV-VI compounds to the BaF_2 substrate, pronounced interference fringes appear in conventional absorption spectra. Therefore, we have developed an important approach for the determination of the absorption of materials placed inside a high-finesse microcavity structure with a small mode spacing by measuring the spectral dispersion of the width of the cavity resonances. The normalized change in resonance width $(w-w_0)/\nu$ was shown to be proportional to the extinction coefficient κ of the cavity material. By applying this method to a microcavity filled with the ordered PbSe quantum dot superlattice, the spectral dependence of the dot absorption could be obtained quantitatively. In particular, the such measured absorption spectrum revealed a narrow peak arising from the dots and a step from the wetting layers. The peak absorption coefficient of the dot ensemble amounts to 2.5×10^4 cm^{-1} and is similar to that of the wetting layers. The assignment of the absorption features was confirmed by calculations of the dispersion of the absorption coefficient using model dielectric functions for 0D quantum dots and 2D wetting layers. The model calculations could be exactly fitted to the experimental data. From this fit, we deduced the interband transition energies of dot and wetting layer as well as the oscillator strengths and the broadening of the optical transitions. The fitted and theoretical values of the oscillator strengths agree very well, especially for the wetting layers with an error of less than 4%. The broadening of the dot transition due to size fluctuations of the quantum dot ensemble was determined to be only 8.7 meV. This is a remarkably small value as compared to other self-assembled quantum dot material systems, evidencing the exceptionally high dot size uniformity in our PbSe quantum dot superlattices, which is a crucial advantage for their application in optoelectronic devices.

ACKNOWLEDGMENTS

The authors thank M. Ratajsky for technical assistance, and M. Aigle and H. Pascher of the University of Bayreuth for helpful discussions. This work was supported by the FWF (Project No. P 13330-TPH) and the GME, Vienna.

*Corresponding author. Email address: thomas.schwarzl@jku.at

[1] Z. Alferov, in *Proceedings of the 25th International Conference on the Physics of Semiconductors*, edited by N. Miura and T. Ando (Springer, Berlin, 2001), p. 14, and references therein.
[2] M. Grundmann *et al.*, Phys. Rev. Lett. **74**, 4043 (1995).
[3] L. Landin, M.S. Miller, M.E. Pistol, C.E. Pryor, and L. Samuelson, Science **280**, 262 (1998).
[4] S. Farad, R. Leon, D. Leonard, J.L. Merz, and P.M. Petroff, Phys. Rev. B **50**, 8086 (1994).
[5] G.T. Liu, H. Li, K.J. Malloy, and L.F. Lester, Electron. Lett. **35**, 1163 (1999).
[6] D. Leonard, M. Krishnamurthy, C.M. Reeves, S.P. Denbaars, and P.M. Petroff, Appl. Phys. Lett. **63**, 3203 (1993).
[7] J. Tersoff and R.M. Tromp, Phys. Rev. Lett. **70**, 2782 (1993).
[8] G. Park, O.B. Shchekin, S. Csutak, D.L. Huffaker, and D.G. Deppe, Appl. Phys. Lett. **75**, 3267 (1999).
[9] S. Farad, K. Hinzer, S. Raymond, M. Dion, J. McCaffrey, Y. Feng, and S. Charbonneau, Science **274**, 1350 (1996).
[10] J. Tersoff, C. Teichert, and M.G. Lagally, Phys. Rev. Lett. **76**, 1675 (1996).
[11] V.A. Shchukin, N.N. Ledentsov, P.S. Kop'ev, and D. Bimberg, Phys. Rev. Lett. **75**, 2968 (1995).
[12] N.N. Ledentsov *et al.*, Phys. Rev. B **54**, 8743 (1996).
[13] G. Springholz, Z. Shi, and H. Zogg, in *Thin Films: Heteroepitaxial Systems*, edited by W.K. Liu and M.B. Santos (World Scientific, Singapore, 1999), p. 621.
[14] G. Springholz, V. Holy, M. Pinczolits, and G. Bauer, Science **282**, 734 (1998).
[15] M. Pinczolits, G. Springholz, and G. Bauer, Phys. Rev. B **60**, 11 524 (1999).
[16] G. Springholz, M. Pinczolits, P. Mayer, V. Holy, G. Bauer, H.H. Kang, and L. Salamanca-Riba, Phys. Rev. Lett. **84**, 4669 (2000).
[17] V. Holy, G. Springholz, M. Pinczolits, and G. Bauer, Phys. Rev. Lett. **83**, 356 (1999).
[18] G. Bauer, M. Kriechbaum, Z. Shi, and M. Tacke, J. Nonlinear Opt. Phys. Mater. **4**, 181 (1995).
[19] D.L. Partin, IEEE J. Quantum Electron. **24**, 1716 (1988).
[20] M. Tacke, Infrared Phys. Technol. **36**, 447 (1995).
[21] M. Tacke, in *Long Wavelength Infrared Emitters Based on Quantum Wells and Superlattices*, edited by M. Helm (Gordon and Breach, Amsterdam, 2000), p. 347.
[22] K. Alchalabi, D. Zimin, H. Zogg, and W. Buttler, IEEE Electron Device Lett. **22**, 110 (2001), and references therein.
[23] M. Helm, in *Long Wavelength Infrared Emitters Based on Quantum Wells and Superlattices* (Ref. 21), p. 1.
[24] J. Faist, F. Capasso, D.L. Sivco, C. Sitori, A.L. Hutchinson, and A.Y. Cho, Science **264**, 553 (1994).
[25] C.L. Felix, W.W. Bewley, I. Vurgraftman, L.J. Olafsen, D.W. Stokes, J.R. Meyer, and M.J. Yang, Appl. Phys. Lett. **75**, 2876 (1999).
[26] P.C. Findlay *et al.* Phys. Rev. B **58**, 12 908 (1998).
[27] T. Schwarzl, W. Heiss, and G. Springholz, Appl. Phys. Lett. **75**, 1246 (1999).
[28] C. Weisbuch, M. Nishioka, A. Ishikawa, and Y. Arakawa, Phys. Rev. Lett. **69**, 3314 (1992).
[29] J.L. Jewell, J.P. Harbinson, A. Scherer, Y.H. Lee, and L.T. Florez, IEEE J. Quantum Electron. **27**, 1332 (1991).
[30] T. Schwarzl, W. Heiss, G. Springholz, M. Aigle, and H. Pascher, Electron. Lett. **36**, 322 (2000).

[31] G. Springholz, T. Schwarzl, M. Aigle, H. Pascher, and W. Heiss, Appl. Phys. Lett. **76**, 1807 (2000).
[32] W. Heiss, T. Schwarzl, G. Springholz, K. Biermann, and K. Reimann, Appl. Phys. Lett. **78**, 862 (2001).
[33] G. Springholz, T. Schwarzl, W. Heiss, G. Bauer, M. Aigle, H. Pascher, and I. Vavra, Appl. Phys. Lett. **79**, 1225 (2001).
[34] H. Krenn, S. Yuan, N. Frank, and G. Bauer, Phys. Rev. B **57**, 2393 (1998).
[35] A. Lipovskii *et al.*, Appl. Phys. Lett. **71**, 3406 (1997).
[36] A. Olkhovets, R.-C. Hsu, A. Lipovskii, and F.W. Wise, Phys. Rev. Lett. **81**, 3539 (1998).
[37] H. Krenn, W. Herbst, H. Pascher, Y. Ueta, G. Springholz, and G. Bauer, Phys. Rev. B **60**, 8117 (1999).
[38] G. Springholz and G. Bauer, Appl. Phys. Lett. **62**, 2399 (1993).
[39] T. Schwarzl, W. Heiss, G. Kocher-Oberlehner, and G. Springholz, Semicond. Sci. Technol. **14**, L11 (1999).
[40] A.F. Terzis, X.C. Liu, A. Petrou, B.D. McCombe, M. Dutta, H. Shen, D.D. Smith, M.W. Cole, M. Taysing-Lara, and P.G. Newman, J. Appl. Phys. **67**, 2501 (1990).
[41] S. Yuan, G. Springholz, G. Bauer, and M. Kriechbaum, Phys. Rev. B **49**, 5476 (1994).
[42] S. Yuan, H. Krenn, G. Springholz, and G. Bauer, Phys. Rev. B **47**, 7213 (1993).
[43] H.Z. Wu, N. Dai, M.B. Johnson, P.J. McCann, and Z.S. Shi, Appl. Phys. Lett. **78**, 2199 (2001).
[44] Q. Xie, A. Madhukar, P. Chen, and N.P. Kobayashi, Phys. Rev. Lett. **75**, 2542 (1995).
[45] H. Krenn (unpublished).
[46] W.-Y. Wu, J.N. Schulman, T.Y. Hsu, and U. Efron, Appl. Phys. Lett. **51**, 710 (1987).
[47] J.-Y. Marzin, J.-M. Gerard, A. Izrael, D. Barrier, and G. Bastard, Phys. Rev. Lett. **73**, 716 (1994).
[48] G.S. Solomon, J.A. Trezza, A.F. Marshall, and J.S. Harris, Jr., Phys. Rev. Lett. **76**, 952 (1996).
[49] P. Frigeri, A. Bosacchi, S. Franchi, P. Allegri, and V. Avanzini, J. Cryst. Growth **201/202**, 1136 (1999).
[50] M. Colocci, A. Vinattieri, L. Lippi, F. Bogani, M. Rosa-Clot, S. Taddei, P. Frigeri, A. Bosacchi, and S. Franchi, Appl. Phys. Lett. **74**, 564 (1999).
[51] K. Kamath, N. Chervela, K.K. Linder, T. Sosnowski, H.-T. Jiang, T. Norris, J. Singh, and B. Bhattacharya, Appl. Phys. Lett. **71**, 927 (1997).
[52] P. Yu *et al.*, Phys. Rev. B **60**, 16 680 (1999).
[53] P. Schittenhelm, C. Engel, F. Findeis, G. Abstreiter, A.A. Darhuber, G. Bauer, A.O. Kosogov, and P. Werner, J. Vac. Sci. Technol. B **16**, 1575 (1998).
[54] V.L. Thanh, V. Yam, Y. Zheng, and D. Bouchier, Thin Solid Films **380**, 2 (2000).
[55] S. Mackowski, G. Karczewski, T. Wojtowicz, J. Kossut, S. Kret, A. Szczepanska, P. Dluzewski, G. Prechtl, and W. Heiss, Appl. Phys. Lett. **78**, 3884 (2001).
[56] R. Houdre, R.P. Stanley, U. Oesterle, M. Ilegems, and C. Weisbuch, Phys. Rev. B **49**, 16 761 (1994).